LANGMUIR Article
Cite This: Langmuir XXXX, XXX, XXX−XXX
pubs.acs.org/Langmuir

# Zwitterionic Cross-Linked Biodegradable Nanocapsules for Cancer Imaging

Haotian Sun,[†] Lingyue Yan,[‡] Kevin A. Carter,[‡] Jiaqi Zhang,[†] Julia S. Caserto,[†] Jonathan F. Lovell,[‡] Yun Wu,*[,‡] and Chong Cheng*[,†]

[†]Department of Chemical and Biological Engineering and [‡]Department of Biomedical Engineering, University at Buffalo, The State University of New York, Buffalo, New York 14260, United States

Supporting Information

**ABSTRACT:** Zwitterionic cross-linked biodegradable nanocapsules (NCs) were synthesized for cancer imaging. A polylactide (PLA)-based diblock copolymer with two blocks carrying acetylenyl and allyl groups respectively was synthesized by ring-opening polymerization (ROP). Azide−alkyne "click" reaction was conducted to conjugate sulfobetaine (SB) zwitterions and fluorescent dye Cy5.5 onto the acetylenyl-functionalized first block of the diblock copolymer. The resulting copolymer with a hydrophilic SB/Cy5.5-functionalized PLA block and a hydrophobic allyl-functionalized PLA block could stabilize miniemulsions because of its amphiphilic diblock structure. UV-induced thiol−ene "click" reaction between a dithiol cross-linker and the hydrophobic allyl-functionalized block of the copolymer at the peripheral region of nanoscopic oil nanodroplets in the miniemulsion generated cross-linked polymer NCs with zwitterionic outer shells. These NCs showed an average hydrodynamic diameter ($D_h$) of 136 nm. They exhibited biodegradability, biocompatibility and high colloidal stability. *In vitro* study indicated that these NCs could be taken up by MIA PaCa-2 cancer cells. *In vivo* imaging study showed that, comparing to a small molecule dye, NCs had a longer circulation time, facilitating their accumulation at tumors for cancer imaging. Overall, this work demonstrates the applicability of zwitterionic biodegradable polymer-based materials in cancer diagnosis.

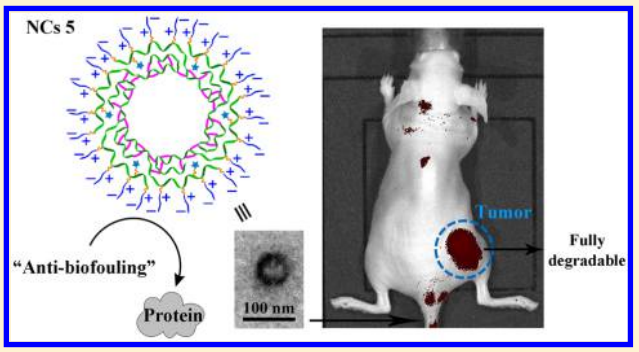


## INTRODUCTION

Polymer nanocapsules (NCs) are polymer nanoparticles (NPs) with inner cavities.[1] Their special hollow core structure makes them promising for various applications such as drug delivery and controlled release of various cargoes.[2,3] Cross-linked NCs have drawn significant attention because their covalently cross-linked shell architectures effectively enhance their structural stability.[4] Robust cross-linked NCs have been employed as containers with persistent structures for therapeutic delivery (including drugs,[5,6] genes,[7] and proteins[8]), medical imaging,[9,10] and "nanoreactors".[11]

Cross-linked NCs can be prepared by the cavitation of preprepared shell-cross-linked nanostructures, vesicular cross-linking, and emulsion-based interfacial cross-linking.[4] The emulsion-based approaches often just require relatively simple components and allow the direct in situ encapsulation of cargos. More specifically, miniemulsions can be employed as templates for preparing cross-linked NCs.[12] For instance, we demonstrated the preparation of cross-linked NCs by highly efficient UV-induced thiol−ene "click" cross-linking of precursor polymers with surfactant properties in transparent miniemulsions in our previous studies.[5,13,14] By using amine-functionalized cationic polylactide (PLA) as the precursor polymer, cationic NCs with well-defined covalently stabilized biodegradable structures were obtained, and *in vitro* studies showed that they can overcome multidrug resistance and enable the individual and codelivery of drugs and genes to cancer cells.[13,15] Moreover, other features of these cationic NCs, such as biodegradability and biocompatibility, also enhance their promising applicability to therapeutic delivery.[16]

Recently, zwitterionic materials have been widely studied for biological applications mainly because of their biocompatibility and antibiofouling properties, which can enable a long blood circulation time.[17,18] The incorporation of biodegradability with zwitterionic materials can minimize their long-term side effects in biological environments, and this is important for enhancing their biomedical applicability.[19] However, most of the reported zwitterionic materials were derived from zwitterionic (meth)acrylic esters or amides and therefore do not possess biodegradability. Taking advantage of the thiol−ene click chemistry using a biodegradable PLA-based precursor

Special Issue: Zwitterionic Interfaces: Concepts and Emerging Applications

Received: May 16, 2018
Revised: July 9, 2018
Published: August 7, 2018






DOI: 10.1021/acs.langmuir.8b01633
Langmuir XXXX, XXX, XXX−XXX

**Scheme 1. (a) Synthesis of PLA-Based Diblock Copolymer 4 with a Hydrophilic SB/Cy5.5-Functionalized Block and a Hydrophobic Allyl-Functionalized Block and (b) Transformation of 4 into Cross-Linked NCs (5)**

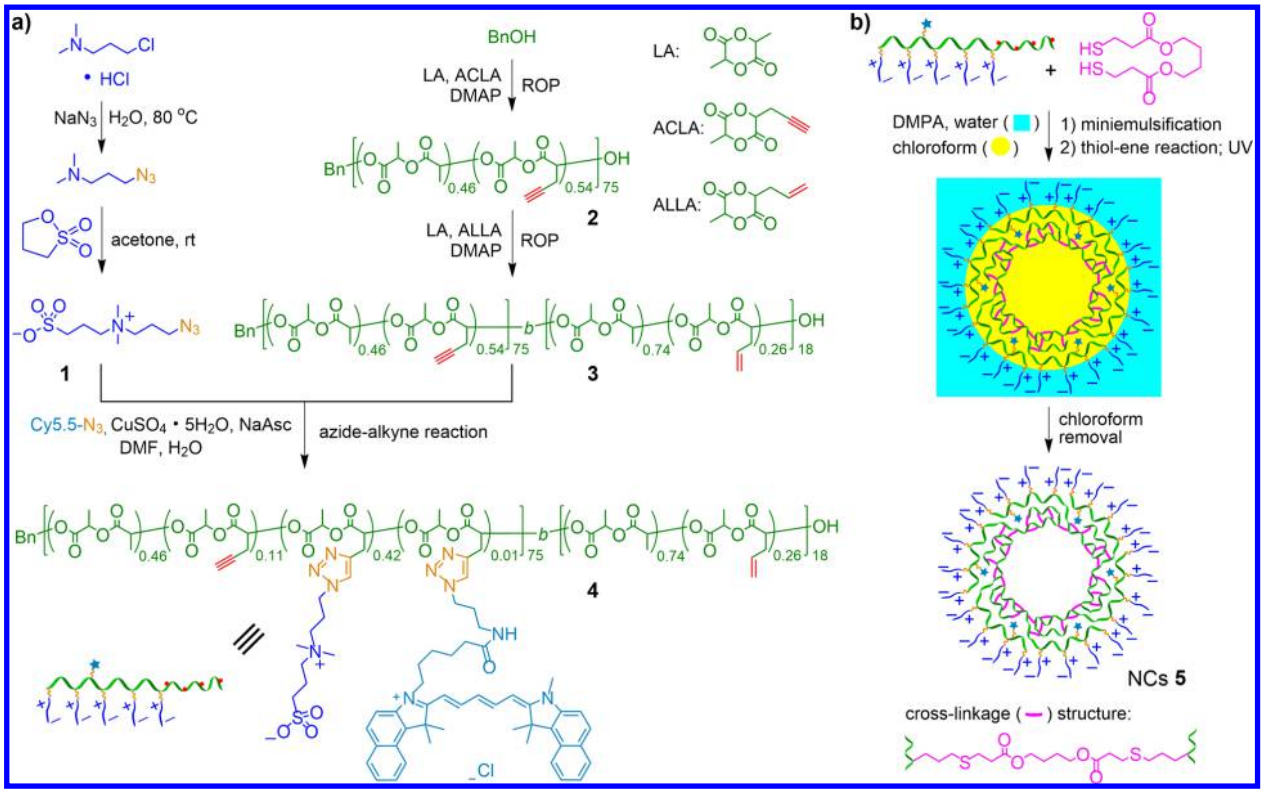


polymer, we recently reported a fully degradable zwitterionic polymer prepared by the thiol−ene reaction of a thiol-functionalized sulfobetaine (SB) zwitterion with allyl-functionalized PLA.[20] The conjugate of the SB-functionalized zwitterionic PLA with paclitaxel, a potent anticancer drug, was also studied for sustained drug delivery.

Fluorescent-dye-doped NPs have attracted significant attention for biomedical imaging applications because they are brighter and more photostable than conventional organic fluorescent probes.[21] Similar to drug delivery systems, NPs for biomedical imaging also need thoughtful design considerations with respect to the structure and properties of the scaffolds, according to the required biological environments.[22] In principle, the unique combination of biomedically relevant properties of zwitterionic biodegradable polymers makes them to be promising scaffold materials for biomedical imaging. Herein, we report novel fluorescent-dye-doped cross-linked NCs derived from zwitterionic SB-functionalized PLAs for cancer imaging (Scheme 1). Besides the favorable properties from the zwitterionic biodegradable precursor polymer, such NCs were designed to have not only nanoscopic dimensions for capitalizing on the enhanced permeability and retention (EPR) effect which leads to the accumulation of NCs at tumor sites but also inner cavities which potentially can be utilized for the delivery of therapeutic cargos. A special SB zwitterion modified with an azide group (SB-$N_3$, **1**) was designed and synthesized. Functional PLAs, including acetylenyl-functionalized PLA **2** and diblock PLA **3** with both acetylenyl- and allyl-functionalized blocks, were prepared successively by ring-opening polymerization (ROP). The azide−alkyne click reaction of **1** and cyanine5.5 azide (Cy5.5-$N_3$), an azide-modified fluorescent dye, with the acetylenyl-functionalized first block of **3** was performed to yield **4** with both SB and Cy5.5 conjugated to its first block.[23] Then **4** was used to prepare NCs by miniemulsion cross-linking via the UV-induced thiol−ene click reaction. The resulting NCs **5** species were demonstrated to be promising cancer imaging agents with high colloidal stability, biodegradability, and biocompatibility. An *in vivo* imaging and biodistribution study also demonstrated that **5** could be used for cancer imaging.

## EXPERIMENTAL SECTION

**Materials.** 3-Dimethylamino-1-propyl chloride hydrochloride (98%) and 1,3-propane sultone (99%) were purchased from Alfa Aesar. Sodium azide (99%), 2,2-dimethoxy-2-phenylacetophenone (DMPA, 99%), and sodium periodate (99%) were purchased from Acros Organics. Magnesium sulfate anhydrous ($MgSO_4$), sodium hydroxide (NaOH, pellets), L-ascorbic acid sodium salt (NaAsc), and copper sulfate pentahydrate ($CuSO_4{\cdot}5H_2O$) were purchased from Fisher Scientific. (3*S*)-*cis*-3,6-Dimethyl-1,4-dioxane-2,5-dione (LA, 98%), 4-(dimethylamino)pyridine (DMAP, 99%, prilled), and fibrinogen from human plasma were purchased from Sigma-Aldrich. Benzyl alcohol (BnOH) was purchased from J. T. Baker. Cy5.5-$N_3$ was purchased from Lumiprobe Corporation. 1,4-Butanediol bis(3-mercaptopropionate) was purchased from Fujifilm Wako Chemical Corporation. Ruthenium dioxide (99.9%) was purchased from Pfaltz & Bauer. Fetal bovine serum (FBS, qualified, USDA-approved regions) was purchased from Life Technologies. Hexanes (HPLC grade), ethyl acetate (HPLC grade), dichloromethane (DCM, HPLC grade), chloroform (HPLC grade), methanol (HPLC grade), diethyl ether (HPLC grade), acetone (Certified ACS grade), and *N*,*N*′-dimethylformamide (DMF, HPLC grade) were purchased from Fisher Scientific. DCM and DMF were dried by distillation over $CaH_2$ before use. Acetylenyl-functionalized lactide (ACLA) and allyl-functionalized lactide (ALLA) were freshly synthesized following the methods reported in our previous publications.[14,24]



DOI: 10.1021/acs.langmuir.8b01633
*Langmuir* XXXX, XXX, XXX−XXX

**Synthesis of 3-Azido-*N*,*N*-dimethylpropan-1-amine.** The reaction was conducted according to the literature with some changes.[25,26] To a round-bottomed flask equipped with a reflux condenser was added 3-dimethylamino-1-propyl chloride hydrochloride (1.58 g, 10.0 mmol, 1.00 equiv), sodium azide (1.30 g, 20.0 mmol, 2.00 equiv), and 20 mL of $H_2O$. The solution was held at 80 °C for 23 h. After the solution cooled to room temperature, 1 M NaOH was added slowly until the solution reached a pH of ∼10. Then the solution was extracted with diethyl ether three times. The organic layers were collected, combined, and dried with $MgSO_4$. After evaporation, the pure product was obtained as a colorless oil (0.84 g, 65% yield). (***Caution!****Because organic azides can be explosive, the reaction must be conducted very carefully.*) $^1$H NMR (500 MHz, $CDCl_3$, $\delta$): 3.34 (t, 2H, $CH_2CH_2CH_2N_3$), 2.34 (t, 2H, $CH_2CH_2CH_2N_3$), 2.22 (s, 6H, $N(CH_3)_2$), 1.75 (m, 2H, $CH_2CH_2CH_2N_3$).

*Synthesis of SB-$N_3$ (**1**).* The reaction was conducted according to the literature with some changes.[20] In a 10 mL glass vial, 1,3-propane sultone (362 mg, 2.97 mmol, 0.95 equiv) was dissolved in 3 mL of dry acetone under a nitrogen atmosphere. Then 3-azido-*N*,*N*-dimethylpropan-1-amine (400 mg, 3.12 mmol, 1.00 equiv) was slowly added to the solution. After a few minutes, white solid powders started to appear in the solution. The mixture was stirred at room temperature for 46 h in total. After filtration, the solid was washed with a large amount of acetone. After drying under vacuum, the pure product was finally obtained as a white solid (0.60 g, 80%). $^1$H NMR (500 MHz, $D_2O$, $\delta$): 3.43−3.28 (m, 6H, $SO_3CH_2CH_2CH_2$ and $CH_2CH_2CH_2N_3$), 3.01 (s, 6H, $N(CH_3)_2$), 2.87 (t, 2H, $SO_3CH_2CH_2CH_2$), 2.17−2.07 and 2.01−1.91 (m, 4H, $SO_3CH_2CH_2CH_2$ and $CH_2CH_2CH_2N_3$).

*Synthesis of Acetylenyl-Functionalized PLA (**2**).* ROP of LA (348 mg, 2.42 mmol) with ACLA (610 mg, 3.63 mmol) was conducted by using BnOH (13.1 mg, 0.12 mmol) as the initiator and DMAP (59.1 mg, 0.48 mmol) as the organocatalyst in dry DCM ($[LA]_0/[ACLA]_0/[BnOH]_0/[DMAP]_0$ = 20:30:1:4). The reaction mixture was stirred for 5 days under a $N_2$ atmosphere at 35 °C. The product was precipitated twice in large amounts of cold methanol to remove the unreacted monomer and the DMAP organocatalyst. Finally, polymer **2** was obtained as a white solid (0.60 g, 63%). $^1$H NMR analysis indicated the formula of **2** to be poly($LA_{0.46}$-*co*-$ACLA_{0.54}$)$_{75}$. $^1$H NMR (500 MHz, $CDCl_3$, $\delta$): 7.41−7.31 (m, Ar−*H* from BnOH), 5.45−5.06 (br m, $CHCH_3$ of LA units; $CHCH_3$, $CHCH_2C{\equiv}CH$ of ACLA units), 3.02−2.66 (br m, $CHCH_2C{\equiv}CH$ of ACLA units), 2.15−1.99 (br s, $CHCH_2C{\equiv}CH$ of ACLA units), 1.67−1.40 (br m, $CHCH_3$ of LA and ACLA units). $M_n^{NMR}$ = 11.9 kDa, $M_n^{GPC}$ = 24.9 kDa, and $Đ^{GPC}$ = 1.10.

*Synthesis of Acetylenyl/Allyl-Functionalized Diblock PLA (**3**).* ROP of LA (66 mg, 0.46 mmol) with ALLA (92 mg, 0.54 mmol) was conducted with copolymer **2** (158 mg, 0.0133 mmol) as the polymeric initiator and DMAP (6.5 mg, 0.053 mmol) as the organocatalyst in dry DCM ($[LA]_0/[ALLA]_0/[\mathbf{2}]_0/[DMAP]_0$ = 34.5:40.5:1:4). The reaction mixture was stirred for 8 days under a $N_2$ atmosphere at 35 °C. The product was precipitated twice in large amounts of cold methanol to remove the unreacted monomers and the DMAP organocatalyst. Finally, diblock polymer **3** was obtained as a white solid (114 mg, 36% yield). $^1$H NMR analysis indicated the formula of **3** to be poly($LA_{0.46}$-*co*-$ACLA_{0.54}$)$_{75}$-*b*-poly($LA_{0.74}$-*co*-$ALLA_{0.26}$)$_{18}$. $^1$H NMR (500 MHz, $CDCl_3$, $\delta$): 7.41−7.31 (m, Ar−*H* from BnOH), 5.91−5.69 (m, $CH_2CH{=}CH_2$ of ALLA units), 5.45−5.05 (br m, $CHCH_3$ of LA units; $CHCH_3$, $CHCH_2C{\equiv}CH$ of ACLA units; $CHCH_3$, $CHCH_2CH{=}CH_2$ of ALLA units), 3.05−2.75 (br m, $CHCH_2C{\equiv}CH$ of ACLA units), 2.75−2.47 (br m, $CHCH_2CH{=}CH_2$ of ALLA units), 2.14−1.99 (br s, $CHCH_2C{\equiv}CH$ of ACLA units), 1.78−1.39 (br m, $CHCH_3$ of LA, ACLA, and ALLA units). $M_n^{NMR}$ = 14.6 kDa, $M_n^{GPC}$ = 28.3 kDa, and $Đ^{GPC}$ = 1.09.

*Synthesis of SB/Cy5.5/Allyl-Functionalized Diblock PLA (**4**).* The azide−alkyne click reaction was conducted to conjugate both SB-$N_3$ and Cy5.5-$N_3$ onto the PLA backbone of **3**. The feed ratio was [acetylenyl group of **3**]$_0$/[SB-$N_3$]$_0$/[Cy5.5-$N_3$]$_0$/[$CuSO_4{\cdot}5H_2O$]$_0$/[NaAsc]$_0$ = 40.5:38.3:1.0:1.8:3.6. A mixture of DMF and $H_2O$ (v/v = 8:1) was used as the reaction solvent. In a 10 mL flask, **3** (72.3 mg) and Cy5.5-$N_3$ (3.4 mg) were added with 4.0 mL of DMF; SB-$N_3$ (47.4 mg) and NaAsc (3.5 mg) were added with 0.4 mL of water. Then the flask was filled with $N_2$, followed by the addition of $CuSO_4{\cdot}5H_2O$ (2.2 mg) with 0.1 mL of $H_2O$ using a syringe. Three freeze−pump−thaw cycles were performed to remove more oxygen in the reaction system. The reaction mixture was stirred for 21 h at room temperature. The crude product was dialyzed against acetone and DCM/MeOH (v/v = 5:1), respectively, to remove the unreacted SB-$N_3$ and Cy5.5-$N_3$. Product **4** (112 mg, 94.4% yield) was obtained as a blue solid after filtration, followed by drying under vacuum. $^1$H NMR (500 MHz, $CDCl_3/CD_3OD$ (v/v 1:1), $\delta$): 8.08−7.72 (br m, $CHCH_2C{=}CHN$), 7.38−7.27 (m, Ar−*H* from BnOH), 5.88−5.69 (br m, $CHCH_2CH{=}CH_2$ of ALLA units), 5.57−5.35 (br m, $CHCH_2C{=}CHN$), 5.34−4.92 (br m, $CHCH_3$, and $CHCH_2CH{=}CH_2$ of ALLA units; $CHCH_3$ of LA and ACLA units), 4.58−4.42 (br m, $NCH_2CH_2CH_2N(CH_3)_2$), 3.66−3.20 (br m, $NCH_2CH_2CH_2N(CH_3)_2$, $NCH_2CH_2CH_2SO_3$, and $CHCH_2C{=}CHN$), 3.18−3.01 (br m, $NCH_2CH_2CH_2N(CH_3)_2$), 2.93−2.76 (br m, $NCH_2CH_2CH_2SO_3$, and $CHCH_2C{\equiv}CH$ of ACLA units), 2.76−2.55 (br m, $CHCH_2CH{=}CH_2$ of ALLA units), 2.53−2.35 (br m, $NCH_2CH_2CH_2N(CH_3)_2$), 2.20−2.04 (br m, $NCH_2CH_2CH_2SO_3$), 2.04−1.96 (br s, $CHCH_2C{\equiv}CH$ of ACLA units), 1.65−1.35 (br m, $CH_3$ of units on the PLA backbone). $M_n^{NMR}$ = 24.7 kDa.

*Synthesis of Cross-Linked SB/Cy5.5-Functionalized PLA-Based NCs (**5**).* In an 8 mL vial, a chloroform solution (0.057 mL) containing 1,4-butanediol bis(3-mercaptopropionate) (0.70 mg, with 1.3 equiv of thiol groups) and DMPA (0.12 mg, 0.1 equiv) was added to 2.83 mL of a water solution of **4** (21.9 mg with 1.0 equiv of allyl groups). Ultrasonication (Branson Sonifier 250, output 1, duty cycle 50%) was performed for 20 min to generate a transparent oil-in-water (O/W) miniemulsion. Then UV irradiation ($\lambda_{max}$ = 365 nm) was conducted for 30 min at room temperature to induce a thiol−ene cross-linking reaction. Finally, the aqueous solution of cross-linked SB/Cy5.5-functionalized NCs ([Cy5.5] = 0.2 mg/mL) was obtained after the removal of chloroform using a rotavapor. During the synthesis process, samples were taken after each step for nanoparticle tracking analysis (NTA) to monitor the size change.

**Characterization Methods.** $^1$H NMR spectra were recorded using a 500 MHz Varian Inova-500 spectrometer at 25 °C with $CDCl_3$ (with tetramethylsilane as an internal standard), $D_2O$, or $CD_3OD$ as the solvent. Gel permeation chromatography (GPC) was used to determine the number-average molecular weight ($M_n$) and molecular weight dispersity ($Đ$) of functionalized PLAs **2** and **3**. A Viscotek GPC system equipped with a VE-1122 pump, a VE-3580 refractive index (RI) detector, and a VE-3210 UV/vis detector was employed. Two mixed-bed organic columns (PAS-103M-UL and PAS-105M-M) were used in the GPC system, with DMF containing 0.01 M LiBr as the eluent (flow rate 0.5 mL/min at 55 °C). Both **2** and **3** were dissolved in DMF to a concentration of ∼3 mg/mL, and the injection volume was 0.1 mL for each measurement. Linear polystyrene standards ($Đ$ < 1.1) purchased from Varian were used for calibration. NTA was used to determine the hydrodynamic diameters ($D_h$) of assembled NPs of **4** and cross-linked NCs of **5**.[27] The measurements were performed on a NanoSight LM10 (Malvern Instruments, laser wavelength 405 nm). Brownian motions of the NPs and the NCs (1 mg/mL) in different aqueous environments were recorded and tracked, from which the size data of each sample were generated. Transmission electron microscopy (TEM) images of assembled NPs of **4** and cross-linked NCs of **5** were obtained with a JEOL 2010 microscope. Their dilute solutions in water (0.1 mg/mL) were dip coated onto the 400-mesh carbon-coated copper TEM grids. After complete drying under vacuum, the samples were stained with a freshly prepared 0.5% solution of ruthenium tetroxide ($RuO_4$). The staining agent was prepared by the reaction between ruthenium dioxide and sodium periodate in water for 1 h. The staining process lasted for 3 h before measurements.

**Cell Culture.** MIA PaCa-2 ATCC CRL-1420 (PaCa-2 for short) cells were purchased from the American Type Culture Collection (Manassas, VA). PaCa-2 cells were cultured in DMEM supplemented with 10% fetal bovine serum (FBS, Life Technologies), 1% penicillin−


DOI: 10.1021/acs.langmuir.8b01633
*Langmuir* XXXX, XXX, XXX−XXX

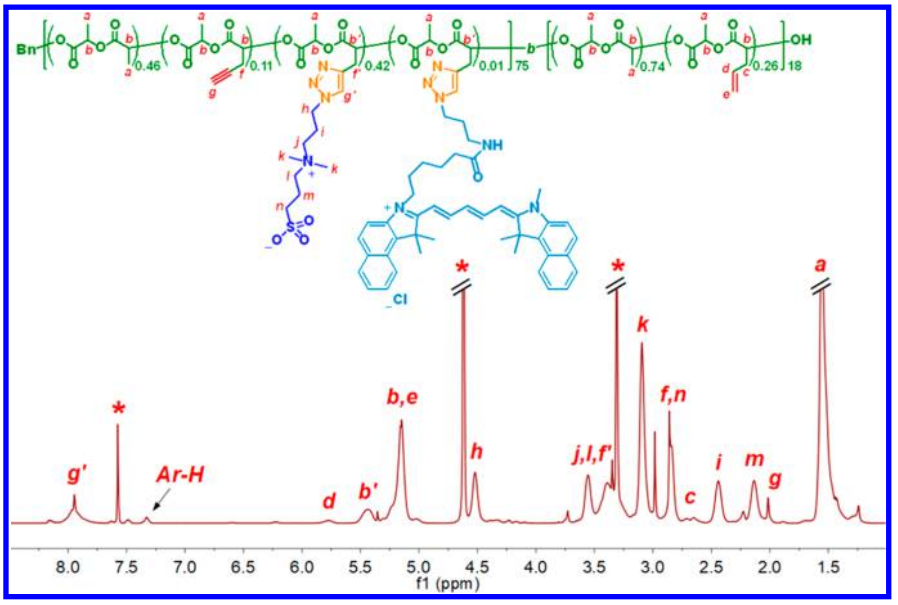


**Figure 1.** $^1$H NMR spectrum of **4** in $CDCl_3/CD_3OD$ (v/v 1:1).

streptomycin and 1% sodium pyruvate (Invitrogen, 11360070) at 37 °C with 5% $CO_2$.

**In Vitro Cell Viability.** The cytotoxicity of NCs of **5** was evaluated on the basis of the viability of PaCa-2 cells. The cells were seeded in 96-well plates (Greiner Bio-one, 655180) at a seeding density of $1 \times 10^4$ cells per well in 100 $\mu$L of cell culture medium. The cells were allowed to grow overnight at 37 °C with 5% $CO_2$. The solutions of NCs of **5** at different concentrations were prepared in cell culture medium to treat cells at final concentrations of 50, 75, 100, 200, 300, and 500 $\mu$g/mL. AlamarBlue (Invitrogen, DAL1025) was used to measure the viability of PaCa-2 cells at 72 h after treatment following the manufacturer's protocol. Briefly, 1 part of the alamarBlue reagent was added to 10 parts of the cell culture medium. The mixture was then added to cells and incubated at 37 °C for 3 h, protected from light. The fluorescence intensity was measured using a TECAN microplate reader (San Jose, CA). The excitation and emission wavelengths were set at 560 and 590 nm, respectively. The cell viability was normalized to that of PBS-treated groups.

**In Vitro Cellular Uptake Analysis.** PaCa-2 cells were seeded in six-well plates (Greiner Bio-one, 657160) at $2 \times 10^5$ cells per well and allowed to grow overnight. The cells were then treated with Cy5.5-$N_3$ and NCs **5** at a Cy5.5 concentration of 0.2 $\mu$g/mL. Untreated cells were the controls. At 24 h post-treatment, the cells were harvested and fixed in 4% paraformaldehyde (Acros, 41678-5000) for analysis by flow cytometry and confocal microscopy. The flow cytometry analysis was conducted with a BD Fortessa flow cytometer (BD Bioscience, San Jose, CA) in the APC channel ($\lambda_{ex}$ = 640 nm and $\lambda_{em}$ = 660 nm). For each sample, 10 000 events were collected. The mean fluorescence intensity ± standard deviation of Cy5.5 was reported to illustrate cellular uptake. For confocal microscopy imaging, the cell nuclei were counterstained with DAPI (Sigma-Aldrich, D8417). Then the cells were mounted on glass slides and imaged using an LSM 710 confocal microscope (ZEISS, Dublin, CA) through the DAPI channel ($\lambda_{ex}$ = 405 nm and $\lambda_{em}$ = 497.5 nm) and Cy5 channel ($\lambda_{ex}$ = 640 nm and $\lambda_{em}$ = 701.5 nm), respectively.

**In Vivo Imaging and Biodistribution.** At the flank of each of the female athymic nude mice (6 weeks old, Charles River Laboratories), $5 \times 10^6$ PaCa-2 cells were injected subcutaneously. When the tumor volume reached ~300 mm$^3$, the mice were divided into three groups and treated with either 0.9% saline (control), Cy5.5-$N_3$ in 0.9% saline, or NCs **5** in 0.9% saline through intravenous injection at a Cy5.5 dose of 1.5 mg/kg of body weight. Whole body Cy5.5 fluorescent images ($\lambda_{ex}$ = 675 nm and $\lambda_{em}$ = 720 nm) were taken with an IVIS Lumina II *in vivo* imaging system (PerkinElmer, Waltham, MA) before injection and 5 min, 1 h, 4 h, and 24 h after injection.[28] Then the mice were euthanized. Tumor and major organs (including brain, heart, liver, spleen, lungs, and kidneys) were harvested. The fluorescent images of organs were recorded and quantified by using the IVIS *in vivo* imaging system. The animal protocol was approved by the University at Buffalo Institutional Animal Care and Use Committee (IACUC).

## RESULTS AND DISCUSSION

**Synthesis and Chemical Characterization.** The synthesis of cross-linked SB/Cy5.5-functionalized PLA-based NCs is illustrated in Scheme 1. An azide-functionalized small-molecule zwitterion, SB-$N_3$ (**1**), was prepared *via* a two-step organic synthesis in which the nucleophilic substitution reaction of 3-dimethylamino-1-propyl chloride with sodium azide was performed first, followed by the reaction of the resulting 3-azido-*N*,*N*-dimethylpropan-1-amine with 1,3-propane sultone. Compound **1** was obtained with an overall yield

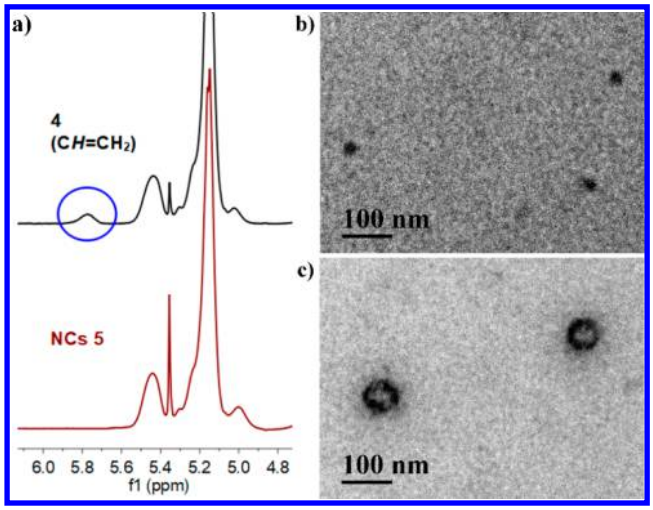


**Figure 2.** (a) Partial $^1$H NMR spectra of **4** and NCs **5** in $CDCl_3/CD_3OD$ (v/v 1:1). (b) TEM image of NPs of **4**. (c) TEM image of NCs **5**. TEM samples were stained with $RuO_4$ before measurements.


DOI: 10.1021/acs.langmuir.8b01633
Langmuir XXXX, XXX, XXX−XXX

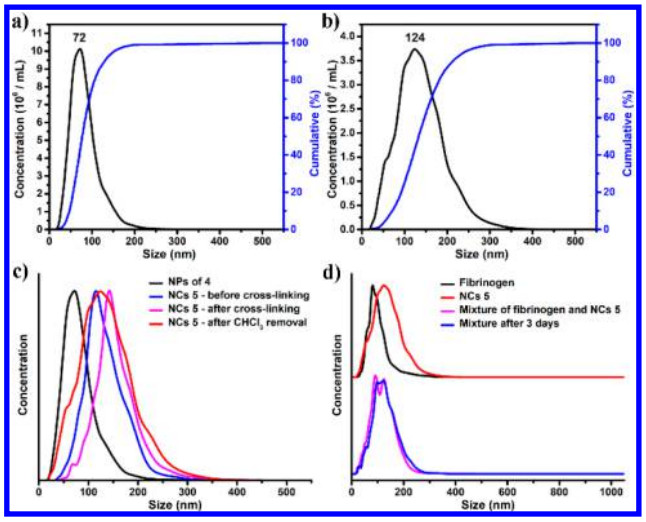


**Figure 3.** Size distribution profiles based on NTA measurements: (a) NPs of **4** in $H_2O$. (b) NCs **5** in $H_2O$. (c) NCs **5** in different steps of the synthesis. (d) Fibrinogen, NCs **5**, and the mixture of these two before incubation and after 3 days of incubation.

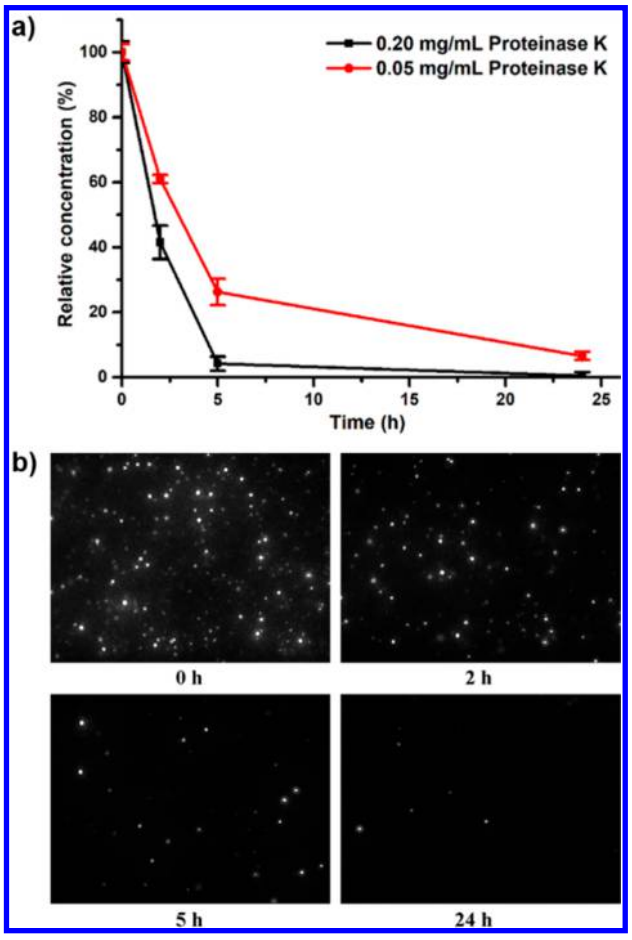


**Figure 4.** (a) Enzymatic degradation profiles of NCs **5** in 0.1 M Tris-HCl buffer (pH 8.5) in the presence of 0.05 and 0.20 mg/mL of proteinase K at 37 °C. (b) NanoSight images of NCs **5** in 0.1 M Tris-HCl buffer (pH 8.5) in the presence of 0.05 mg/mL of proteinase K at 37 °C at different times.

of 52%, and its high purity was illustrated by $^1$H NMR analysis (Figure S1).

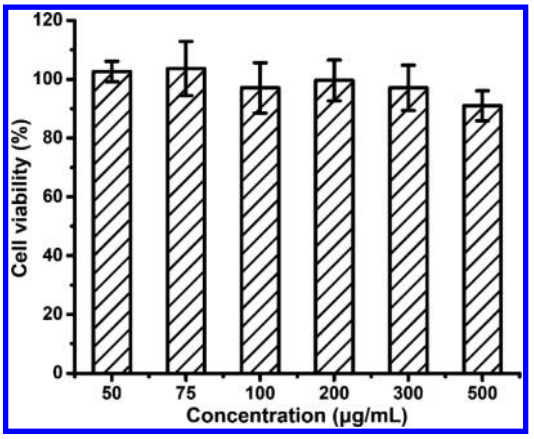


**Figure 5.** Cytotoxicity of NCs **5** in PaCa-2 cells. PaCa-2 cells were treated with NCs **5** at concentrations of 50, 75, 100, 200, 300, and 500 $\mu$g/mL. The cell viability was measured at 72 h post-treatment, and normalized to PBS treated controls ($n$ = 3).

The diblock PLA backbone (**3**) was synthesized by a two-step ROP process. Relative to a one-step ROP process with sequential additions of monomers, the two-step ROP process can allow us to access strictly defined diblock structures because incomplete monomer conversion for the preparation of the first block would not affect the synthesis of the second block. The first step was ROP of LA and ACLA initiated by BnOH and organocatalyzed by DMAP at 35 °C for 5 days ($[LA]_0/[ACLA]_0/[BnOH]_0/[DMAP]_0$ = 20:30:1:4) to give acetylenyl-functionalized PLA **2** in 63% yield after purification. $^1$H NMR analysis revealed that **2** was composed of 46 mol % LA and 54 mol % ACLA (Figure S2a), according to the areas of peak b (COOC*H* of LA and ACLA units) at 5.06−5.45 ppm, peak f ($CHCH_2C{\equiv}CH$ of ACLA units) at 2.66−3.02 ppm, and peak g ($CHCH_2C{\equiv}CH$ of ACLA units) at 1.99−2.15 ppm. The total degree of polymerization (DP) of 75 was determined for **2** (40.5 for ACLA units, 34.5 for the LA unit) on the basis of the comparison of the area of peak b with the area of the peak for Ar−H (from the terminal Bn group) at 7.31−7.41 ppm. The second step was ROP of LA with ALLA using **2** as the initiator and DMAP as the organocatalyst at 35 °C for 8 days ($[LA]_0/[ALLA]_0/[\mathbf{2}]_0/[DMAP]_0$ = 34.5:40.5:1:4). Diblock functional PLA **3** was obtained in 36% yield after purification, and the relatively low yield was ascribed to the decreased reactivity of active polymer terminals with the increase in the polymer chain length. According to $^1$H NMR analysis, the allyl-functionalized second PLA-based block of **3** was composed of 74 mol % LA and 26 mol % ACLA (Figure S2b). The number of ALLA units was determined to be 4.6 by comparing the areas of peak d ($CH_2CH{=}CH_2$ of the ALLA units) and peak g ($CHCH_2C{\equiv}CH$ of the ACLA units) on the basis of the assumption that the first acetylenyl-functionalized block of **3** was identical to precursor **2** regarding chain length and composition. Then the number of LA units in the second block was determined to be 13.5 by comparing the areas of peak d ($CH_2CH{=}CH_2$ of units from ALLA) and peak a ($CHCH_3$ of the LA units from both blocks; $CHCH_3$ of 4.6 ALLA units and 40.5 ACLA units). Thus, with a DP of 18 for its second block, diblock copolymer **3** had an overall DP of 93. GPC analysis revealed well-controlled chain growth and extension in the ROP process, and polymers **2** and **3** had low$Đ$ values of 1.10 and 1.09, respectively, relative to that of linear polystyrenes (Figure S3).



DOI: 10.1021/acs.langmuir.8b01633
*Langmuir* XXXX, XXX, XXX−XXX

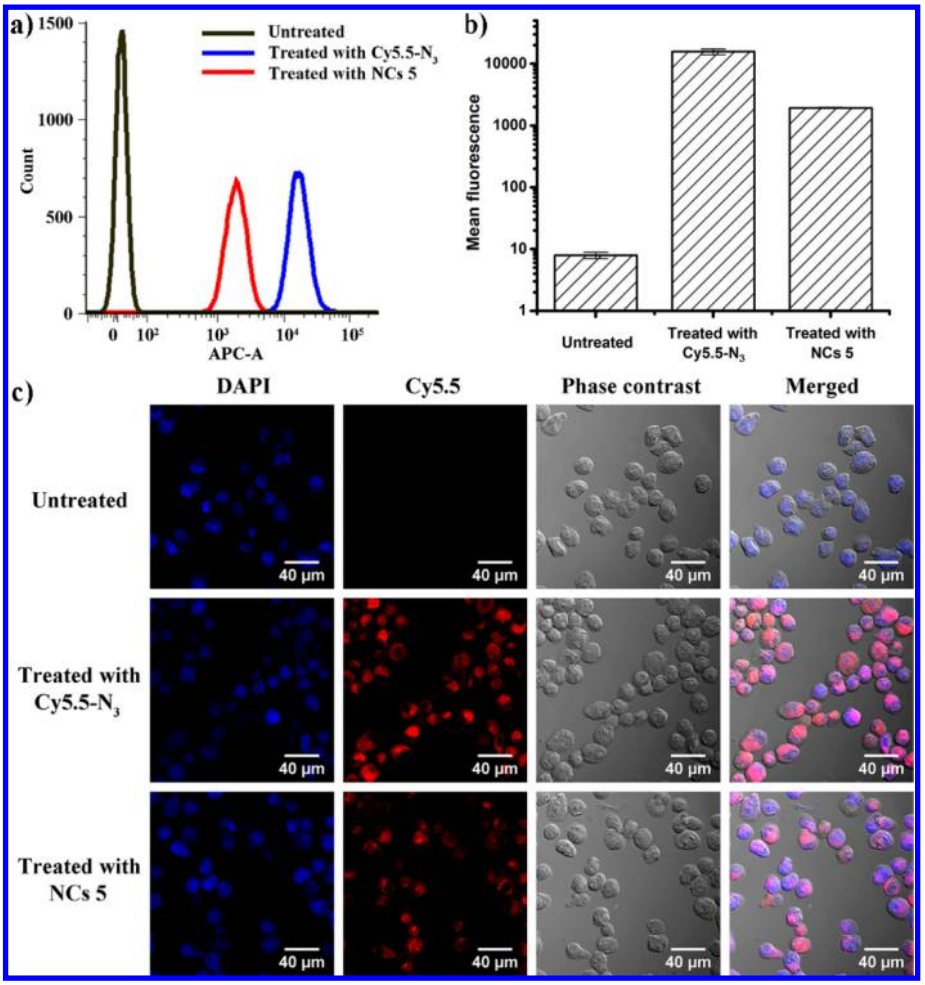


**Figure 6.** (a) Typical set of flow cytometry data showing the uptake of Cy5.5-$N_3$ and NCs **5** in PaCa-2 cells at 24 h post-treatment. (b) Mean fluorescence intensity of Cy5.5 obtained from flow cytometry ($n$ = 3). (c) Confocal microscopy images of PaCa-2 cells at 24 h post-treatment with Cy5.5-$N_3$ and NCs **5**. Cell nuclei were counterstained with DAPI.

Highly efficient azide−alkyne click chemistry was employed to react both SB-$N_3$ (**1**) and Cy5.5-$N_3$ with acetylenyl groups of **3** using $CuSO_4{\cdot}5H_2O$/NaAsc as the catalytic system in DMF/$H_2O$ (v/v = 8:1) mixed solvent at room temperature for 21 h ($[\text{acetylenyl group of } \mathbf{3}]_0/[\text{SB-N}_3]_0/[\text{Cy5.5-N}_3]_0/[CuSO_4{\cdot}5H_2O]_0/[\text{NaAsc}]_0$ = 40.5:38.3:1.0:1.8:3.6). After the azide−alkyne reaction, the reaction solution was analyzed by DMF GPC. Resulting diblock copolymer **4** with a hydrophilic SB/Cy5.5-functionalized PLA block and a hydrophobic allyl-functionalized PLA block showed very low solubility in DMF because of its amphiphilic property,[20,29] and only a very weak GPC curve of the crude product of **4** was observed with an RI detector (Figure S3b). On the other hand, the more visible GPC peak of **4** obtained with a UV/vis detector (wavelength of 684 nm) indicated the presence of the conjugated Cy5.5 moiety in **4** as a result of the successful azide−alkyne conjugation reaction (Figure S3b). A comparison of the UV/vis signal intensity of **4** to that of unreacted Cy5.5-$N_3$ indicated ∼67% conversion of Cy5.5-$N_3$ in the reaction, which should be a lower limit of conversion because Cy5.5-$N_3$ is more soluble than **4** in DMF. After separation by dialysis, **4** was obtained in 94.4% yield based on the mass of the recovered polymer. $^1$H NMR analysis revealed 31.3 wt % SB moieties in **4** (Figure 1), corresponding to 74% conversion of SB-$N_3$ in the azide−alkyne reaction. The number of SB conjugated ACLA units per molecule of **4** was determined to be 31.1 by comparing the areas of peak Ar−H (from Bn) with peak i ($NCH_2CH_2CH_2N(CH_3)_2$ from units of SB). The number was also confirmed by comparing the areas of peak Ar−H and peak g ($CHCH_2C{\equiv}CH$ from units of ACLA). Meanwhile, according to the intensities of the $^1$H NMR resonances from allyl protons, $^1$H NMR analysis indicated that allyl groups from **3** were completely intact during the azide−alkyne reaction and therefore were available for the synthesis of NCs *via* thiol−ene cross-linking.

Amphiphilic diblock PLA **4** can effectively stabilize the water−oil interface because its hydrophilic SB/Cy5.5-functionalized block and hydrophobic allyl-functionalized block can effectively affiliate with water and oil phases, respectively. A transparent miniemulsion was readily obtained by ultrasonication of a mixture consisting of water (∼98 vol %), chloroform (as oil, ∼2 vol %), **4**, 1,4-butanediol bis(3-mercaptopropionate) (as a dithiol cross-linker), and DMPA (as a photoinitiator) for 20 min ($[\text{thiol}]_0/[\text{allyl of } \mathbf{4}]_0/[\text{DMPA}]_0$ = 1.3:1.0:0.1). Subsequently, the thiol−ene cross-linking reaction was performed by UV irradiation ($\lambda_{max}$ = 365 nm) of the transparent miniemulsion for 30 min, converting **4** to cross-linked SB/Cy5.5-functionalized PLA-based NCs **5**. A sample of the final NCs solution was freeze-dried and analyzed by $^1$H NMR. The absence of the resonance of the C*H* proton


DOI: 10.1021/acs.langmuir.8b01633
*Langmuir* XXXX, XXX, XXX−XXX

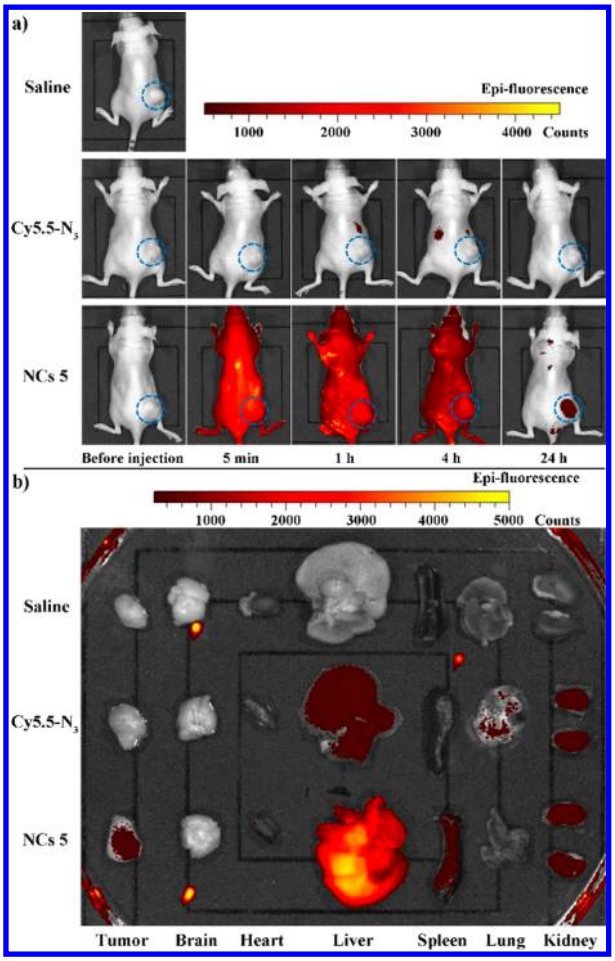


**Figure 7.** (a) Whole body fluorescence imaging of mice (dorsal side) before injection and at different time points after the intravenous injection of saline, Cy5.5-$N_3$, and NCs **5** at a Cy5.5 dose of 1.5 mg/kg body weight. Tumors are circled in each panel. (b) *Ex vivo* fluorescence imaging of tumors and major organs at 24 h after the intravenous injection of saline, Cy5.5-$N_3$, and NCs **5**.

from allyl groups at 5.88−5.69 ppm confirmed that all of the allyl groups were consumed during the thiol−ene reaction process, forming cross-linked structures (Figure 2a). Although in principle the dithiol cross-linker can also react with the remaining acetylenyl groups on the hydrophilic SB/Cy5.5-functionalized block under UV irradiation, as evidenced by the remaining resonances of acetylenyl protons in the $^1$H NMR spectrum of **5** (Figure S4), the thiol−yne reaction was not important in the current case for several reasons. First, allyl groups are much more reactive than acetylenyl groups toward thiols *via* the radical reaction mechanism.[30] Second, these acetylenyl groups remained after azide−alkyne functionalization reactions that are generally associated with significant steric hindrance. Third, the local concentration of the hydrophobic dithiol cross-linker can be relatively low around the hydrophilic SB/Cy5.5-functionalized blocks with the remaining acetylenyl groups.

**Nanostructure Characterization.** Nanostructures were involved for both SB/Cy5.5/allyl-functionalized diblock PLA **4** and the derived cross-linked NCs **5**. While NCs **5** possesses covalently stabilized unimolecular nanostructure, amphiphilic diblock PLA **4** forms nanoparticles (NPs) through self-assembly in selective solvents. The assembled NPs of **4** and cross-linked NCs **5** were characterized by both NTA and TEM to reveal their structural features. Dynamic light scattering (DLS) was not employed in this study because the excitation and emission spectra of Cy5.5 can interfere with the 4 mW 633 nm laser of the Zetasizer Nano ZS90 (Malvern Instruments Ltd.).[31] NTA showed that NPs of **4** had an average hydrodynamic diameter ($D_h$) of 84 nm (with the peak of the profile at 72 nm) (Figure 3a). The size of NPs of **4** was larger than a previously reported zwitterionic sulfobetaine polymer (hydrodynamic diameter: 14.4 ± 0.1 nm) without amphiphilic diblock structure.[20] The TEM image of NPs of **4** showed spherical NPs with a number-average diameter of 38.2 ± 2.3 nm (Figure 2b). For NCs **5**, NTA showed an average hydrodynamic diameter ($D_h$) of 136 nm (with the peak of the profile at 124 nm) (Figure 3b), which was larger than that of NPs of **4** (Figure 3c). TEM images of NCs **5** confirmed the morphology of these NCs as spherical NPs with inner cavities (Figure 2c, Figure S5). The number-average diameter of NCs **5** was determined to be 92.1 ± 18.4 nm. The larger size of NCs **5** relative to that of NPs of **4** was a result of employing miniemulsion templates in the preparation of **5**. The dissolution of the hydrophobic allyl-functionalized block of **4** by the dispersed oil phase of the miniemulsion led to a much larger interfacial area per oil nanodroplet of the miniemulsion than the interfacial area per NP of **4** in its aqueous dispersion. Thus, on average, each NCs **5** obtained from miniemulsion cross-linking corresponds to more molecules of **4** than each of the assembled NPs of **4**. The presence of the inner cavity of **5** also contributes to the larger average outer dimension of **5** as compared to that of NPs of **4**.

It is noteworthy that NTA was also used to monitor the miniemulsion cross-linking synthesis of NCs **5** (Figure 3c). Before cross-linking, the average $D_h$ of oil nanodroplets stabilized by **4** was 135 nm. After cross-linking, the average $D_h$ of oil nanodroplets encapsulated by NCs **5** was 157 nm. After the removal of chloroform, the final NCs **5** dispersed in water showed an average $D_h$ of 136 nm. The fact that the nanodroplets and the resulting NCs **5** exhibited similar dimensions indicates well-controlled template synthesis.

**Assessment of Nonspecific Interactions of NCs 5 with Biomolecules.** The surface layer of NCs **5** contains superhydrophilic zwitterionic SB moieties. Because of the hydration effects of these zwitterionic materials, NCs **5** was expected to have low nonspecific interactions with biomolecules.[17,32] In this study, fibrinogen (from human plasma) was chosen as the model biomolecule, which is a glycoprotein that is essential to the formation of fibrin-based blood clots.[20,33] NTA showed that fibrinogen (1 mg/mL in $H_2O$) itself had a mean $D_h$ of 105 nm (with the peak of the profile at 81 nm). A mixture of fibrinogen (1 mg/mL in $H_2O$) and NCs **5** (1 mg/mL in $H_2O$) showed a bimodal profile, with the two peaks corresponding to fibrinogen and NCs **5** (Figure 3d). In addition, no large particles could be detected immediately after mixing, indicating that no aggregates formed during the mixing process. The mixture was allowed to stand for 3 days at room temperature. After 3 days, an NTA measurement showed almost the same size profile. The aforementioned results all indicated that the nonspecific interaction between fibrinogen and NCs **5** was well suppressed.

**Evaluation of the Stability of NCs 5 in Serum.** Serum is the clear liquid separated from clotted blood that includes all proteins not involved in blood clotting (fibrinogens not included) and special components such as antibodies,


DOI: 10.1021/acs.langmuir.8b01633
*Langmuir* XXXX, XXX, XXX−XXX

hormones, and antigens. During the blood circulation of nanocarriers, serum may trigger aggregation and shorten their circulation time. The stability of NCs **5** in fetal bovine serum (FBS, 50% in PBS buffer) was evaluated by monitoring the size change.[34] As shown in Figure S6a, NTA had a size profile of NCs **5** in 50% FBS (average $D_h$: 136 nm) similar to that in $H_2O$. After the incubation of NCs **5** in 50% FBS at 37 °C for 3 days, the size profile remained essentially unchanged (average $D_h$: 138 nm), indicating the high stability of the NCs **5** in serum. While the cross-links effectively maintained NCs **5** as an integrated nanostructure, the nonfouling SB moieties on the surface domain of NCs **5** helped suppress the nonspecific interaction between NCs **5** and various components from serum and prevent aggregation.

**Biodegradation of NCs 5.** The biodegradation behavior of NCs **5** was investigated by NTA assessment of the Tris-HCl buffer solutions (0.1 M, pH 8.5) of 1 mg/mL NCs **5** in the presence of proteinase K (0.05 and 0.2 mg/mL), which were incubated in a shaking bed at 37 °C. Quick degradation was illustrated by the fast decreases in the relative concentration of **5** as the number ratio of the individual NCs per unit volume detected by NTA at a given time versus the initial time (Figure 4). The degradation rate positively depended on the enzyme concentration, indicating that the degradation was catalyzed by the enzyme and therefore was a biodegradation process. In the presence of 0.2 mg/mL of proteinase K enzyme, the biodegradation of **5** was essentially complete within 24 h. Related to the current study, the studies of biodegradation behaviors of SB-functionalized PLA (i.e., the structural analogue of the hydrophilic block of **4** and the pendant hydrophilic chains on NCs **5**) and thiol−ene-cross-linked PLA-based NCs (with the cross-linked domains similar to that of NCs **5**) were reported in our previous publications.[14,20]

It should be clarified that NCs **5** showed remarkable stability in aqueous solutions without the presence of a catalytic enzyme. No significant changes in the hydrodynamic size of **5** could be observed by storing a deionized water solution of **5** at room temperature for 80 days (Figure S7). The results indicated the covalent stabilization effect of the cross-linked structures of **5** and suggested an insignificant hydrolytic degradation rate of **5** under typical storage conditions.

**In Vitro Cytotoxicity Study.** Both PLA and zwitterions were commonly considered to be materials with high biocompatibility.[35,36] The cytotoxicity of NCs **5** in PaCa-2 pancreatic cancer cells was evaluated by the alamarBlue cell viability assay at 72 h against post-treatment of PaCa-2 pancreatic cancer cells (Figure 5). The results showed that NCs **5** (up to 500 $\mu$g/mL) was nontoxic in PaCa-2 cells, indicating the high biocompatibility of these imaging agents.

**In Vitro Cellular Uptake Study.** NCs **5** and Cy5.5-$N_3$ showed comparable profiles of fluorescence intensity versus Cy5.5 concentration in solutions (Figure S8), indicating that NCs **5** are not fluorescently self-quenched compared to the free dye and therefore the Cy5.5 moieties on NCs **5** can serve as effective fluorescent probes. PaCa-2 cells were treated with Cy5.5-$N_3$ and NCs **5** at a Cy5.5 concentration of 0.2 $\mu$g/mL. Untreated cells were the controls. At 24 h post-treatment, the cellular uptake of NCs **5** in PaCa-2 cells was characterized quantitatively with flow cytometry and qualitatively with confocal microscopy. Flow cytometry data showed that NCs **5** were effectively taken up by PaCa-2 cells (Figure 6a). The mean fluorescence intensity of cells treated with NCs **5** was ∼243-fold higher than that of untreated cells (Figure 6b). Confocal microscopy images also confirmed that NCs **5** were successfully taken up by PaCa-2 cells and accumulated inside the cells (Figure 6c). Cy5.5-$N_3$-treated cells showed stronger fluorescence signals than NCs **5**, which agreed well with previously published work.[31] Although Cy5.5-$N_3$ showed better cellular uptake efficiency *in vitro*, it mainly accumulated in the liver and was not able to reach tumor sites *in vivo*, which is described in detail below.

**In Vivo Imaging and Biodistribution.** PaCa-2 cells were injected subcutaneously into the flanks of 6-week-old female athymic nude mice. When the tumors reached ∼300 $mm^3$, the mice were injected with 0.9% saline (control group), Cy5.5-$N_3$, or NCs **5** intravenously at a Cy5.5 dose of 1.5 mg/kg body weight. Whole body fluorescence imaging using the IVIS *in vivo* imaging system was performed before injection and 5 min, 1 h, 4 h, and 24 h post injection to investigate the biodistributions of Cy5.5-$N_3$ and NCs **5**. For the mice injected with NCs **5**, as shown in Figure 7a, NCs **5** were distributed across the whole mouse body (dorsal side) immediately after injection. After 4 h, fluorescence signals could still be detected throughout the mouse's body, suggesting that NCs **5** circulated during the first 4 h after injection. At 24 h post injection, from the dorsal side of the mice, only the tumors showed fluorescence signals, indicating that NCs **5** successfully accumulated at tumor sites. For the mice injected with Cy5.5-$N_3$, images of both the dorsal side (Figure 7a) and the ventral side (Figure S9) of the mice were taken using the IVIS imaging system.[37] At 5 min post injection, from the dorsal side, no fluorescence signal was detected, and the image from the ventral side showed strong fluorescence signals in the liver, suggesting the immediate clearance of Cy5.5-$N_3$ by the liver. At 1 and 4 h post injection, more accumulation of Cy5.5-$N_3$ in the liver (seen from the ventral side) and kidneys (seen from the dorsal side) was observed, indicating the continuous clearance of Cy5.5-$N_3$ by the liver and kidneys. Within the 24 h imaging period, no fluorescence signal was ever detected at tumor sites.

Mice were euthanized 24 h after injection. Tumors and major organs were harvested and imaged with the IVIS imaging system (Figure 7b). Besides in the liver, spleen, and kidneys, significant fluorescence signals were observed in the tumors of NCs **5**-treated mice, indicating that NCs **5** were effective imaging agents for PaCa-2 tumors. In contrast, there was no accumulation of free Cy5.5-$N_3$ in the tumors, while fluorescence signals were observed in the liver and kidneys.

The above *in vivo* imaging and biodistribution results indicated that SB/Cy5.5-functionalized NCs **5** exhibited a longer circulation time *in vivo* and led to more effective tumor accumulation than the small-molecule dye, Cy5.5-$N_3$. Both nanoscopic dimensions of NCs **5** and the zwitterionic properties of **5**, which promote the colloidal stability of **5** under biological environments, are contributing factors to such results.[38,39] With their hydrodynamic size of ∼100 nm, the accumulation of NCs **5** at tumor sites was ascribed to the EPR effect. The intensive fluorescence signals from the liver and noticeable fluorescence signals from the spleen suggested that the reticuloendothelial system (RES) might play a major role in the clearance of NCs **5** because of RES clearance.[40] The fluorescence signals from the kidneys suggested renal clearance of the population of NCs **5** with relatively small sizes or degraded residues of **5** because renal clearance mainly functions for objects with a size smaller than ∼10 nm.[41] For the mice treated with free Cy5.5-$N_3$, the significant


DOI: 10.1021/acs.langmuir.8b01633
*Langmuir* XXXX, XXX, XXX−XXX

accumulation of Cy5.5-$N_3$ in kidneys and liver indicates that both renal clearance and liver uptake are significant pathways to eliminating the dye molecules. Because renal clearance *via* kidney prefers objects with small sizes, the dye molecules cleared through liver uptake were likely due to larger particles. The lower fluorescence intensity in the liver of Cy5.5-$N_3$-treated mice relative to that of NCs **5**-treated mice might be due to the degradation of a small-molecule dye in the liver. It is noteworthy that because the NPs of **4** are different from NCs **5** with respect to the hydrodynamic size and also have limited structural stability due to their assembled structures, the NPs of **4** were not used as a control in the above studies.

## CONCLUSIONS

SB/Cy5.5-functionalized cross-linked PLA-based NCs were synthesized and characterized. These NCs showed a series of comprehensive biomedically relevant properties, including colloidal stability, biodegradability, biocompatibility, prolonged *in vivo* circulation time, and effective tumor accumulation (as compared to small molecules). The results suggest that NCs are candidate cancer imaging agents. Other properties of these NCs may also be useful for other potential biomedical applications in the future, such as the individual delivery or codelivery of drugs and genes. Although the SB zwitterion was utilized in this work, it should be noted that other zwitterions such as carboxybetaine and phosphorylcholine are also valid options of zwitterions,[42] showing that a broad degree of zwitterionic nanostructures can be generated to explore biomedical applications.

## ASSOCIATED CONTENT

### Supporting Information

The Supporting Information is available free of charge on the ACS Publications website at DOI: 10.1021/acs.langmuir.8b01633.

$^1$H NMR spectra, GPC curves, TEM images, NanoSight curves and data, mean fluorescence profiles, and fluorescence imaging (PDF)

## AUTHOR INFORMATION


### Corresponding Authors

*E-mail: ywu32@buffalo.edu.

*E-mail: ccheng8@buffalo.edu.

### ORCID

Jonathan F. Lovell: 0000-0002-9052-884X

Yun Wu: 0000-0002-6926-777X

Chong Cheng: 0000-0002-4637-1320


### Notes

The authors declare no competing financial interest.

## ACKNOWLEDGMENTS

This work was supported by the U.S. National Science Foundation (DMR-1609914, CHE-1412785, and CBET-1337860) and the U.S. National Institutes of Health (R21 EB024095-01). The authors thank Prof. Mark T. Swihart and Mr. Zheng Fu for their help with NTA measurements, Dr. Yueling Qin for technical support with TEM measurements, and the UB North Campus Confocal Imaging Facility in the Department of Biological Sciences along with their NSF grant (National Science Foundation Major Research Instrumentation grant no. DBI 0923133).

## ABBREVIATIONS

NCs, nanocapsules; NPs, nanoparticles; ROP, ring-opening polymerization; NMR, nuclear magnetic resonance; GPC, gel permeation chromatography; NTA, nanoparticle tracking analysis; TEM, transmission electron microscopy.

## REFERENCES


(1) Meier, W. Polymer nanocapsules. *Chem. Soc. Rev.* **2000**, *29*, 295−303.

(2) Mora-Huertas, C. E.; Fessi, H.; Elaissari, A. Polymer-based nanocapsules for drug delivery. *Int. J. Pharm.* **2010**, *385*, 113−142.

(3) Esser-Kahn, A. P.; Odom, S. A.; Sottos, N. R.; White, S. R.; Moore, J. S. Triggered Release from Polymer Capsules. *Macromolecules* **2011**, *44*, 5539−5553.

(4) Sun, H.; Chen, C.-K.; Cui, H.; Cheng, C. Crosslinked polymer nanocapsules. *Polym. Int.* **2016**, *65*, 351−361.

(5) Chen, C.-K.; Wang, Q.; Jones, C. H.; Yu, Y.; Zhang, H.; Law, W.-C.; Lai, C. K.; Zeng, Q.; Prasad, P. N.; Pfeifer, B. A.; Cheng, C. Synthesis of pH-Responsive Chitosan Nanocapsules for the Controlled Delivery of Doxorubicin. *Langmuir* **2014**, *30*, 4111−4119.

(6) Tian, K.; Zeng, J.; Zhao, X.; Liu, L.; Jia, X.; Liu, P. Synthesis of multi-functional nanocapsules via interfacial AGET ATRP in miniemulsion for tumor micro-environment responsive drug delivery. *Colloids Surf., B* **2015**, *134*, 188−195.

(7) Yan, M.; Wen, J.; Liang, M.; Lu, Y.; Kamata, M.; Chen, I. S. Y. Modulation of Gene Expression by Polymer Nanocapsule Delivery of DNA Cassettes Encoding Small RNAs. *PLoS One* **2015**, *10*, e0127986.

(8) Cheng, R.; Meng, F.; Ma, S.; Xu, H.; Liu, H.; Jing, X.; Zhong, Z. Reduction and temperature dual-responsive crosslinked polymersomes for targeted intracellular protein delivery. *J. Mater. Chem.* **2011**, *21*, 19013−19020.

(9) An, P.; Ba, X.; Lu, S. Preparation and characterization of crosslinked poly(methylmethacrylate) heat sensitive color-developing nanocapsules. *Polym. Bull.* **2010**, *64*, 375−386.

(10) Jagielski, N.; Sharma, S.; Hombach, V.; Mailänder, V.; Rasche, V.; Landfester, K. Nanocapsules Synthesized by Miniemulsion Technique for Application as New Contrast Agent Materials. *Macromol. Chem. Phys.* **2007**, *208*, 2229−2241.

(11) Baier, G.; Musyanovych, A.; Dass, M.; Theisinger, S.; Landfester, K. Cross-linked starch capsules containing dsDNA prepared in inverse miniemulsion as "nanoreactors" for polymerase chain reaction. *Biomacromolecules* **2010**, *11*, 960−968.

(12) Landfester, K. Miniemulsion Polymerization and the Structure of Polymer and Hybrid Nanoparticles. *Angew. Chem., Int. Ed.* **2009**, *48*, 4488−4507.

(13) Chen, C.-K.; Law, W.-C.; Aalinkeel, R.; Yu, Y.; Nair, B.; Wu, J.; Mahajan, S.; Reynolds, J. L.; Li, Y.; Lai, C. K.; Tzanakakis, E. S.; Schwartz, S. A.; Prasad, P. N.; Cheng, C. Biodegradable cationic polymeric nanocapsules for overcoming multidrug resistance and enabling drug-gene co-delivery to cancer cells. *Nanoscale* **2014**, *6*, 1567−1572.

(14) Zou, J.; Hew, C. C.; Themistou, E.; Li, Y. K.; Chen, C. K.; Alexandridis, P.; Cheng, C. Clicking Well-Defined Biodegradable Nanoparticles and Nanocapsules by UV-Induced Thiol-Ene Cross-Linking in Transparent Miniemulsions. *Adv. Mater.* **2011**, *23*, 4274−4277.

(15) Sun, H.; Yarovoy, I.; Capeling, M.; Cheng, C. Polymers in the Co-delivery of siRNA and Anticancer Drugs for the Treatment of Drug-resistant Cancers. *Topics Curr. Chem.* **2017**, *375*, 24.

(16) Lin, G.; Hu, R.; Law, W.-C.; Chen, C.-K.; Wang, Y.; Chin, H. L.; Nguyen, Q. T.; Lai, C. K.; Yoon, H. S.; Wang, X.; Xu, G.; Ye, L.; Cheng, C.; Yong, K.-T. Biodegradable Nanocapsules as siRNA Carriers for Mutant K-Ras Gene Silencing of Human Pancreatic Carcinoma Cells. *Small* **2013**, *9*, 2757−2763.

(17) Jiang, S. Y.; Cao, Z. Q. Ultralow-Fouling, Functionalizable, and Hydrolyzable Zwitterionic Materials and Their Derivatives for Biological Applications. *Adv. Mater.* **2010**, *22*, 920−932.




DOI: 10.1021/acs.langmuir.8b01633
*Langmuir* XXXX, XXX, XXX−XXX

(18) Jin, Q.; Chen, Y.; Wang, Y.; Ji, J. Zwitterionic drug nanocarriers: A biomimetic strategy for drug delivery. *Colloids Surf., B* **2014**, *124*, 80−86.
(19) Zheng, L. C.; Sun, Z. J.; Li, C. C.; Wei, Z. Y.; Jain, P.; Wu, K. Progress in biodegradable zwitterionic materials. *Polym. Degrad. Stab.* **2017**, *139*, 1−19.
(20) Sun, H.; Chang, M. Y. Z.; Cheng, W.-I.; Wang, Q.; Commisso, A.; Capeling, M.; Wu, Y.; Cheng, C. Biodegradable zwitterionic sulfobetaine polymer and its conjugate with paclitaxel for sustained drug delivery. *Acta Biomater.* **2017**, *64*, 290−300.
(21) Santra, S.; Dutta, D.; Walter, G. A.; Moudgil, B. M. Fluorescent nanoparticle probes for cancer imaging. *Technol. Cancer Res. Treat.* **2005**, *4*, 593−602.
(22) Barreto, J. A.; O'Malley, W.; Kubeil, M.; Graham, B.; Stephan, H.; Spiccia, L. Nanomaterials: Applications in Cancer Imaging and Therapy. *Adv. Mater.* **2011**, *23*, H18−H40.
(23) Meldal, M.; Tornoe, C. W. Cu-catalyzed azide-alkyne cycloaddition. *Chem. Rev.* **2008**, *108*, 2952−3015.
(24) Yu, Y.; Zou, J.; Yu, L.; Jo, W.; Li, Y. K.; Law, W. C.; Cheng, C. Functional Polylactide-g-Paclitaxel-Poly(ethylene glycol) by Azide-Alkyne Click Chemistry. *Macromolecules* **2011**, *44*, 4793−4800.
(25) Engler, A. C.; Bonner, D. K.; Buss, H. G.; Cheung, E. Y.; Hammond, P. T. The synthetic tuning of clickable pH responsive cationic polypeptides and block copolypeptides. *Soft Matter* **2011**, *7*, 5627−5637.
(26) Zeng, D. Y.; Kuang, G. T.; Wang, S. K.; Peng, W.; Lin, S. L.; Zhang, Q.; Su, X. X.; Hu, M. H.; Wang, H. G.; Tan, J. H.; Huang, Z. S.; Gu, L. Q.; Ou, T. M. Discovery of Novel 11-Triazole Substituted Benzofuro[3,2-b]quinolone Derivatives as c-myc G-Quadruplex Specific Stabilizers via Click Chemistry. *J. Med. Chem.* **2017**, *60*, 5407−5423.
(27) Tian, T.; Zhang, H.-X.; He, C.-P.; Fan, S.; Zhu, Y.-L.; Qi, C.; Huang, N.-P.; Xiao, Z.-D.; Lu, Z.-H.; Tannous, B. A.; Gao, J. Surface functionalized exosomes as targeted drug delivery vehicles for cerebral ischemia therapy. *Biomaterials* **2018**, *150*, 137−149.
(28) Carter, K. A.; Wang, S.; Geng, J. M.; Luo, D. D.; Shao, S.; Lovell, J. F. Metal Chelation Modulates Phototherapeutic Properties of Mitoxantrone-Loaded Porphyrin-Phospholipid Liposomes. *Mol. Pharmaceutics* **2016**, *13*, 420−427.
(29) Cai, M. T.; Leng, M. T.; Lu, A. J.; He, L.; Xie, X. X.; Huang, L.; Ma, Y. H.; Cao, J.; Chen, Y. W.; Luo, X. L. Synthesis of amphiphilic copolymers containing zwitterionic sulfobetaine as pH and redox responsive drug carriers. *Colloids Surf., B* **2015**, *126*, 1−9.
(30) Lowe, A. B., Bowman, C. N., Eds.; Thiol-X chemistries in polymer and materials science*Royal Society of Chemistry*; Polymer Chemistry Series; Royal Society of Chemistry: Cambridge, U.K., 2013.
(31) Garg, S. M.; Paiva, I. M.; Vakili, M. R.; Soudy, R.; Agopsowicz, K.; Soleimani, A. H.; Hitt, M.; Kaur, K.; Lavasanifar, A. Traceable PEO-poly(ester) micelles for breast cancer targeting: The effect of core structure and targeting peptide on micellar tumor accumulation. *Biomaterials* **2017**, *144*, 17−29.
(32) Chen, S. F.; Li, L. Y.; Zhao, C.; Zheng, J. Surface hydration: Principles and applications toward low-fouling/nonfouling biomaterials. *Polymer* **2010**, *51*, 5283−5293.
(33) Wang, L. G.; Yang, Q. H.; Cui, Y. S.; Gao, D. W.; Kang, J. X.; Sun, H. T.; Zhu, L. L.; Chen, S. F. Highly stable and biocompatible dendrimerencapsulated gold nanoparticle catalysts for the reduction of 4-nitrophenol. *New J. Chem.* **2017**, *41*, 8399−8406.
(34) Lin, W.; Ma, G.; Kampf, N.; Yuan, Z.; Chen, S. Development of Long-Circulating Zwitterionic Cross-Linked Micelles for Active-Targeted Drug Delivery. *Biomacromolecules* **2016**, *17*, 2010−2018.
(35) Yu, Y.; Zou, J.; Cheng, C. Synthesis and biomedical applications of functional poly(alpha-hydroxyl acid)s. *Polym. Chem.* **2014**, *5*, 5854−5872.
(36) Zheng, L. C.; Sundaram, H. S.; Wei, Z. Y.; Li, C. C.; Yuan, Z. F. Applications of zwitterionic polymers. *React. Funct. Polym.* **2017**, *118*, 51−61.
(37) Cordero, A. B.; Kwon, Y.; Hua, X.; Godwin, A. K. In vivo Imaging and Therapeutic Treatments in an Orthotopic Mouse Model of Ovarian Cancer. *J. Visualized Exp.* **2010**, 2125.
(38) Wang, B.; He, X.; Zhang, Z. Y.; Zhao, Y. L.; Feng, W. Y. Metabolism of Nanomaterials in Vivo: Blood Circulation and Organ Clearance. *Acc. Chem. Res.* **2013**, *46*, 761−769.
(39) Chen, Y.; Li, Z.; Wang, H.; Wang, Y.; Han, H.; Jin, Q.; Ji, J. IR-780 Loaded Phospholipid Mimicking Homopolymeric Micelles for Near-IR Imaging and Photothermal Therapy of Pancreatic Cancer. *ACS Appl. Mater. Interfaces* **2016**, *8*, 6852−6858.
(40) Petros, R. A.; DeSimone, J. M. Strategies in the design of nanoparticles for therapeutic applications. *Nat. Rev. Drug Discovery* **2010**, *9*, 615−627.
(41) Longmire, M.; Choyke, P. L.; Kobayashi, H. Clearance properties of nano-sized particles and molecules as imaging agents: considerations and caveats. *Nanomedicine* **2008**, *3*, 703−717.
(42) Shao, Q.; Jiang, S. Y. Molecular Understanding and Design of Zwitterionic Materials. *Adv. Mater.* **2015**, *27*, 15−26.


DOI: 10.1021/acs.langmuir.8b01633
*Langmuir* XXXX, XXX, XXX−XXX